A Transversely Isotropic Viscoelastic Constitutive Equation for Brainstem Undergoing Finite Deformation

Xinguo Ning

Qiliang Zhu

Yoram Lanir

Susan S. Margulies[1]

e-mail: margulie@seas.upenn.edu

Department of Bioengineering,
University of Pennsylvania,
Philadelphia, PA 19104-6382

The objective of this study was to define the constitutive response of brainstem undergoing finite shear deformation. Brainstem was characterized as a transversely isotropic viscoelastic material and the material model was formulated for numerical implementation. Model parameters were fit to shear data obtained in porcine brainstem specimens undergoing finite shear deformation in three directions: parallel, perpendicular, and cross sectional to axonal fiber orientation and determined using a combined approach of finite element analysis (FEA) and a genetic algorithm (GA) optimizing method. The average initial shear modulus of brainstem matrix of 4-week old pigs was 12.7 Pa, and therefore the brainstem offers little resistance to large shear deformations in the parallel or perpendicular directions, due to the dominant contribution of the matrix in these directions. The fiber reinforcement stiffness was 121.2 Pa, indicating that brainstem is anisotropic and that axonal fibers have an important role in the cross-sectional direction. The first two leading relative shear relaxation moduli were 0.8973 and 0.0741, respectively, with corresponding characteristic times of 0.0047 and 1.4538 s, respectively, implying rapid relaxation of shear stresses. The developed material model and parameter estimation technique are likely to find broad applications in neural and orthopaedic tissues. [DOI: 10.1115/1.2354208]

Keywords: brain tissues, brainstem, shear, large deformation, viscoelastic, hyperelastic, anisotropic, genetic algorithm, finite element analysis

Introduction

Each year approximately 1.5 million Americans experience traumatic brain injury (TBI), of which 300,000–550,000 die or require hospital admission [1,2]. In children, TBI is the most common cause of death with a hospitalization and death rate of over 200 per 100,000 children [3]. Primary traumatic brain injury occurs in regions experiencing large deformations due to applied force or acceleration, which may be exacerbated near irregular boundaries and constitutive property discontinuities [4–9]. For example, a TBI occurs when brain is exposed to sudden deceleration or acceleration, which produces a shear deformation of brain tissues and may lead to microscopic lesions and degeneration of axonal fibers. The brainstem is a conduit for most cranial nerves and contains the primitive and essential centers of the vasomotor, respiratory, and cardiac systems. Not surprisingly, the brainstem is involved in more than 50% of cases of severe head injuries and more than 70% of those with survival times less than 48 h [10]. Elucidating accurate constitutive response of brainstem undergoing large deformation may lead to better understanding of head injury mechanisms and help establish more effective public safety standards and strategies.

The brainstem consists of bundles of axonal fibers distinctly oriented in a longitudinal direction and embedded in a matrix of extracellular components and oligodendrocytes. Arbogast and Margulies [11,12] tested brainstem at small shear strain (2.5%) and developed a fiber-reinforced composite model based on linear elastic theory. They found brainstem was transversely isotropic viscoelastic at small deformation, but the constitutive response of brainstem undergoing large deformation, associated with severe injury conditions, has yet to be investigated.

Few studies developed the constitutive response of brain tissue undergoing large deformation as an anisotropic, viscoelastic material. Previously, brain tissue was modeled as an isotropic viscoelastic material [13–17] or an anisotropic, hyperelastic material [18]. Recently, Prange and Margulies [19] investigated the regional, directional, and age-dependent properties of adult porcine gray and white matter at large shear deformation using an isotropic, hyper-viscoelastic model. They determined the shear properties of adult porcine tissues separately in two orthogonal directions to evaluate the anisotropy. They found that both corona radiata and corpus callosum demonstrated significant anisotropic behavior. Like brain white matter, brainstem possesses a transversely isotropic structure and demonstrates anisotropic viscoelastic behaviors at small deformation [12]. Therefore, it is reasonable to consider anisotropic viscoelastic characteristics for a constitutive model of brainstem at large deformation.

The overall objective of the present study was to define the constitutive response of brainstem undergoing finite shear deformation. The brainstem was characterized as a transversely isotropic viscoelastic material and the material model was formulated for numerical implementation. Model parameters were fit to shear test data. In these tests, the shear force of 4-week old porcine brainstem specimens were measured in three directions, each defined tangential to the shearing planes: parallel, perpendicular, and cross sectional to axonal fiber orientation as illustrated in Fig. 1. Material parameters were obtained using a novel approach to combine FEA and a GA optimizing method. The research results provided information to understand the vulnerability of brainstem subjected to common rotational loading.

[1]Corresponding author.

Contributed by the Bioengineering Division of ASME for publication in the JOURNAL OF BIOMECHANICAL ENGINEERING. Manuscript received September 15, 2005; final manuscript received June 29, 2006. Review conducted by Ellen M. Arruda. Paper presented at the BMES 2005.

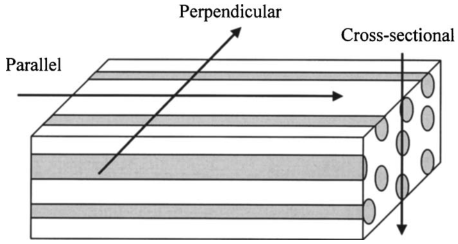

Fig. 1 Schematic diagram of shearing directions relative to axonal fiber orientations

Model Formulation

Based on its anatomy and on previous published data of small strain response [11,12], the brainstem was assumed to be transversely isotropic. Because the brainstem also exhibits time-dependent behavior like most biological soft tissues, in the present study, a transversely isotropic viscoelastic model was developed to describe the response of the brainstem at large shear deformation for numerical implementation. First, we presented the instantaneous response of the brainstem as a transversely isotropic hyperelastic material [20,21]. A specific strain-energy function was established for the brainstem. Next, the instantaneous response was incorporated into a viscoelastic material formulation which was extended from small strains to finite strains using hereditary integrals [22].

Transversely Isotropic Hyperelastic Response of Brainstem. A specific uncoupled strain-energy density function in the form of Eq. (A9) in the Appendix was assumed to depict the individual contribution of the isotropic matrix and axonal fibers for the response of brainstem. For simplicity, neo-Hookean strain-energy function was employed to describe the matrix controlled response of the brainstem

$$W_{\mathrm{iso}}(\tilde{I}_1,\tilde{I}_2,J) = C_{10}(\tilde{I}_1 - 3) + \frac{1}{D_1}(J-1)^2 \tag{1}$$

where C_{10} and D_1 are coefficients. Neo-Hookean strain-energy function is the simplest hyperelastic model and exhibits a constant shear modulus, which uses only linear terms of the invariants in the deviatoric strain energy. Physically, the neo-Hookean potential represents the Helmholtz free energy of a molecular network with Gaussian chain-length distribution [22].

The initial low strain shear modulus G_0 and the bulk modulus K_0 only depend on the coefficients of Eq. (1)

$$G_0 = 2C_{10}, \quad \mathrm{K}_0 = \frac{2}{\mathrm{D}_1} \tag{2}$$

For the additional contribution of axonal fiber reinforcements, a quadratic standard reinforcing strain-energy function [23,24] is used

$$W_{\mathrm{aniso}}(\tilde{I}_4,\tilde{I}_5) = \tfrac{1}{2}\theta(\tilde{I}_4 - 1)^2 \tag{3}$$

where θ defines a measure of the strength of fiber reinforcement; and the effect of I_5 on the strain energy is not considered in the study.

The corresponding deviatoric Cauchy stress and equivalent pressure in Eq. (A17) for this specific constitutive model are

$$\mathbf{S} = \frac{2}{J}\left\{ W_1\tilde{\mathbf{B}} + \tilde{I}_4 W_4 \mathbf{a}\otimes\mathbf{a} - \frac{1}{3}(\tilde{I}_1 W_1 + \tilde{I}_4 W_4)\mathbf{I} \right\} \tag{4}$$

$$p = -\frac{2}{J}\cdot\frac{1}{3}(\tilde{I}_1 W_1 + \tilde{I}_4 W_4) \tag{5}$$

where $W_1 = C_{10}, W_4 = \theta(\tilde{I}_4 - 1)$.

Time-Dependent Response to Large Deformation

In the above analysis, the instantaneous nonlinear elastic response of the brainstem was established. In nature, the brainstem tissue is actually viscoelastic. Thus, the strain or stress field of materials is time dependent. For small deformation, linear isotropic viscoelastic materials may be described using a basic hereditary integral

$$\boldsymbol{\sigma}(t) = \int_0^t 2G(t-t')\dot{\mathbf{e}}dt' + \mathbf{I}\int_0^t K(t-t')\dot{\epsilon}dt' \tag{6}$$

where $\dot{\mathbf{e}}$ and $\dot{\epsilon}$ are the mechanical deviatoric and volumetric strain rate, respectively; K and G are the bulk and shear moduli, respectively, which are the functions of the time t with respect to t'.

A suitable generalization to finite strain of the hereditary integral formulation is obtained as follows [22]:

$$\boldsymbol{\tau}(t) = \boldsymbol{\tau}_0(t) + \mathrm{SYM}\left\{ \int_0^t \mathbf{F}_t^{-1}(t-t')\cdot\left[\frac{\dot{G}(t')}{G_0}\boldsymbol{\tau}_0^D(t-t') + \frac{\dot{K}(t')}{K_0}\boldsymbol{\tau}_0^H(t-t') \right]\cdot\mathbf{F}_t(t-t')dt' \right\} \tag{7}$$

where $\boldsymbol{\tau}$ is the Kirchhoff stress; SYM indicates the symmetrical part of the matrix; $\mathbf{F}_t(t-t')$ is the deformation gradient of the state at $t-t'$ relative to the state at t. It is assumed that the instantaneous response of the material follows from the hyperelastic constitutive equations. $\boldsymbol{\tau}_0^D$ and $\boldsymbol{\tau}_0^H$ are the deviatoric and the hydrostatic parts of the instantaneous Kirchhoff stress $\boldsymbol{\tau}_0$, respectively.

The shear and bulk moduli may be expressed in terms of the time domain Prony series

$$G(t) = G_0\left(g_\infty + \sum_{i=1}^{N_G} g_i e^{-t/\tau_i^G} \right) \tag{8}$$

$$K(t) = K_0\left(k_\infty + \sum_{i=1}^{N_k} k_i e^{-t/\tau_i^K} \right) \tag{9}$$

where g_i and k_i are the relative shear and bulk relaxation moduli of term i, respectively; $g_\infty + \sum_{i=1}^{N_G} g_i = k_\infty + \sum_{i=1}^{N_k} k_i = 1$; it is assumed that the relaxation times $\tau_i = \tau_i^K = \tau_i^G$. Besides, just two terms in the Prony series were considered in the present model. Therefore, there were only two characteristic time parameters: τ_1 and τ_2.

Combining Eqs. (7)–(9), the deviatoric and volumetric parts of the time-dependent stress response of the brainstem can be further separated into two hereditary integrals

$$\boldsymbol{\tau}^H(t) = \boldsymbol{\tau}_0^D(t) - \mathrm{SYM}\left[\sum_i^2 \int_0^t \frac{g_i}{\tau_i}\mathbf{F}_t^{-1}(t-t')\cdot\boldsymbol{\tau}_0^D(t-t')\cdot\mathbf{F}_t(t-t')e^{-t'/\tau_i}dt' \right] \tag{10}$$

$$\boldsymbol{\tau}^H(t) = \boldsymbol{\tau}_0^H(t) - \sum_i^2 \int_0^t \frac{k_i}{\tau_i}\boldsymbol{\tau}_0^H(t-t')e^{-t'/\tau_i}dt' \tag{11}$$

To implement Eqs. (4), (5), (10), and (11) for a transversely isotropic hyper-viscoelastic material, Kirchhoff stress is transformed to Cauchy stress using the relations below

$$\mathbf{S}(t) = \boldsymbol{\tau}^D(t)/J(t) \tag{12}$$

$$p(t) = -\tfrac{1}{3}\mathbf{I}:\boldsymbol{\tau}^H(t)/J(t) \tag{13}$$

The developed material model was programmed and implemented as a subroutine of commercial ABAQUS software/Standard 6.3 (HKS Inc., Pawtucket, RI). The model contained nine material

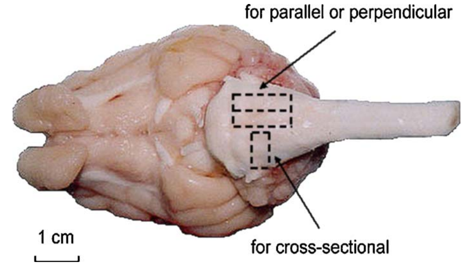

Fig. 2 Anatomic locations of specimens of 4-week old pig brainstem for three shearing directions

parameters, i.e., $C_{10}(=G_0/2)$, $D_1(=2/K_0)$, g_1, g_2, k_1, k_2, θ, τ_1, and τ_2. Like most soft tissues, the brainstem is nearly incompressible. The material bulk modulus is very high and nearly constant over time [25]. For shear deformation, the volume does not change, $J=1$ and the deformation is isochoric. Values of bulk modulus had little effect on the finite shear deformation. In the present study, bulk modulus K_0 was set to be 2 GPa [25], and relative relaxation bulk moduli $k_1=k_2=0$. Thus, the developed transversely isotropic, finite-viscoelastic model was fit to experimental data to determine the six remaining independent parameters: $C_{10}(=G_0/2)$, g_1, g_2, θ, τ_1, and τ_2.

Experiment

Specimen Preparation. Rectangular brainstem specimens (roughly, $10\times5\times1$ mm) were harvested from 4-week old piglets ($n=15$), in a protocol approved by the University of Pennsylvania Institutional Animal Care and Use Committee. Because shear stress relaxation tests were performed in the three principal shearing directions, three specimens were prepared from each pig. The three shearing directions were parallel, perpendicular, and cross sectional to the axonal fiber orientation (Fig. 1). The specimens were excised from the pons of brainstem and their anatomical locations are illustrated in Fig. 2. All specimens were immediately transported in 4°C mock cerebral spinal fluid solution and tested within 5 h postmortem. Before shear testing, the dimensions (length, width, and thickness) of each specimen were measured in triplicate with a digital caliper and then averaged.

Shear Testing. The shear test was done using a custom designed, humidified, parallel-plate shear testing device [26]. The soft, tacky specimen was held in place between two glass plates without adhesive and with negligible precompression. In the test, the shear displacement and force were measured during rapid stress relaxation tests.

For each shearing direction, one specimen was tested at seven different strain levels in the following sequence: 50%, 40%, 30%, 20%, 10%, 5%, and 2.5%. The strain level was defined as $u/2h$ (u was the relative displacement between the two parallel plates; h was the distance between the two plates or the specimen thickness). In order to verify reproducibility, the specimen was tested an eighth time at the strain level of 50% again.

For each strain level, two preconditioning runs were performed to reduce hysteresis, and the third run was recorded as data (1 kHz sampling rate). In each run, one plate was displaced parallel to the other plate with a ramp time of about 40 ms and then held for 60 s. Steady state was verified at 60 s to ensure less than a 0.5% change in stress over the last 5 s. After each run, the specimen was allowed to relax for additional 60 s. For each specimen, force and displacement time histories at each strain level were stored on computer for further numerical analysis.

Experimental Data Quality Assessment. In order to minimize the experimental error, two quality control criteria were established to screen the experiments from 15 animals. Each experiment consisted of three sets of test data for the three test directions and was required to pass both quality control criteria simultaneously in all three test directions.

First, test reproducibility was verified by comparing the first and second 50% shear force measurement in each of the three test directions to ensure no slip between the specimens and glass plates during the measurement at different strain levels. If the second measurement was different from the first, it indicated that the boundary condition of the specimens had been changed by the testing. Specifically, we defined the reproducibility criterion "*Ratio*" in terms of the mean value of the sum of the normalized cross-variance between two measurements

$$\text{Ratio} = \frac{4}{N_t}\sum_{i=1}^{N_t}\left(\frac{F_i^{1\text{st}}-F_i^{2\text{nd}}}{F_i^{1\text{st}}+F_i^{2\text{nd}}}\right)^2 \tag{14}$$

where subscript i represented the ith time point in the force-time history; N_t was the total number of the time points of the time history; F was the experimental shear force; and superscripts 1st and 2nd represented the first and the second results, respectively. Reproducibility was assessed using every time point over the interval including the end of the ramp displacement and beginning of the hold period, when force monotonically increased to the peak force value and then monotonically decreased. To compare $F_i^{1\text{st}}$ and $F_i^{2\text{nd}}$, we must verify similar input displacement for the two measurements. In our tests, the input plate displacement of the second 50% strain level was always within 10% of the first 50% run, averaging $2.3\%\pm2.53\%$ (mean±SD).

If Ratio exceeded 0.05 for any of three directions, indicating the difference between the two force measurements was beyond 20%, none of this animal's data were included for analysis.

Second, the shear test results in the parallel and perpendicular directions were examined for the remaining experiments. Because the brainstem structurally demonstrated transverse isotropy, theoretically at the same strain level the experimental shear stress in the parallel and perpendicular directions should be equal. We used a relation similar to Eq. (14) to evaluate the difference between the test results in the parallel and perpendicular directions. In Eq. (14), shear stress, equal to recorded F divided by the measured area (specimen length × width), was substituted for shear force F.

Parameter Estimation

Since the parameters had to be simultaneously fit to three independent shear test data sets obtained in the three shear orientations, common parameter optimizing routines might become stuck at a local minimum that best fits one or two directions. Besides, the material coefficients were implicitly contained in the closed-form expressions of Eqs. (10) and (11). Thus, numerical solutions were employed to fit material parameters in an iterative process that combined a GA optimizing method with finite element analysis.

Finite Element Model of Brainstem. 3D finite element models were created for each specimen. In each model, the element and node number was the same. The meshing of a specimen was $10\times5\times5$ elements in the directions of length × width × height, respectively, using C3D8 solid elements. A typical 3D finite element model is shown in Fig. 3. All the translational degrees of freedom at each node of the bottom plane were constrained to represent a no-slip boundary between the specimen and the stationary lower plate. On the top plane, the nodes were allowed to move only in the direction of length, simulating a no-slip boundary at the top plate as it was displaced tangentially to the shearing plane. The recorded displacement time histories of the top plate were input to the finite element model as loading conditions.

Genetic Algorithm Method. In numerical methods, GA has been found to be an efficient global optimizing approach based on the principles of "survival of the fittest" and pseudorandom information exchanges [27]. It demonstrates robustness and flexibility

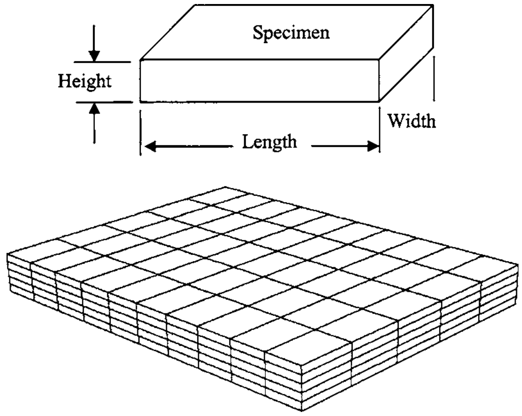

Fig. 3 3D finite element model of brainstem specimen

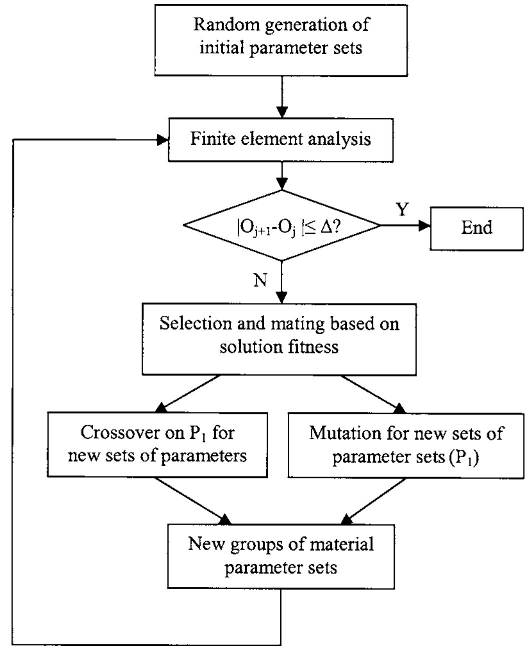

Fig. 4 Flowchart to identify optimal material parameters—a combined approach of finite element analysis and genetic algorithm optimizing method

to solve the problems with discontinuities or local minima encountered in the current study. In fitting the brainstem parameters, our goal is to fit parameters simultaneously to three independent shear test data sets obtained in the three shearing directions. However, common optimizing routines might become stuck at a local minimum that best fits only one or two directions. The genetic algorithm optimizing method is capable of circumventing such difficulties via a set of operations of evaluation, selection, mutation, and crossover.

In the present study, a differential evolution (DE) algorithm [27] was adopted and combined with finite element simulation of the shear tests. A DE, one of the most efficient types of genetic algorithms, is a stochastic, population-based optimization algorithm. Compared with other evolutionary algorithms that typically use mutation for parameter vectors (chromosomes or genomes) themselves, the DE uses the mutations of the differences of the parameter vectors. The DE algorithm requires the user to specify a range encompassing the possible optimal parameters. To ensure that the true optimal value would be in the range specified, ample space surrounding published values in the literature was used. The predefined parameter spaces were: $C_{10} \in [0.001\ 10.0]$ (kPa), $(g_1+g_2) \in (0.0\ 0.999]$, $g_1/(g_1+g_2) \in (0.75\ 0.99]$, $\tau_1 \in [0.001\ 1.0]$ (s), $\tau_2 \in [0.01\ 10.0]$ (s), and $\theta \in [0.01\ 10.0]$ (kPa). In our optimal program, GA searches the values of g_1+g_2 and $g_1/(g_1+g_2)$ and then obtains g_1 and g_2, because in this way it is convenient to apply the constraint condition: $g_1+g_2<1$.

Numerical Implementation. The transversely isotropic viscoelastic material model was programmed and incorporated into ABAQUS/Standard using its user subroutine interface UMAT. In the program, the material parameters and the initial material orientations in the reference configuration were defined as the input variables. In the program, the formulations of the deformation gradient left Cauchy–Green tensor and Cauchy stress can be used directly. The elastic tensors were then extended to finite viscoelasticity by introducing the modulus relaxation function. An explicit integration scheme was used for incremental equations.

A detailed flowchart provides an overview (Fig. 4) of the numerical implementation of the DE genetic algorithm optimization and FEA method to fit the shear test data.

In the first run, the GA randomly assigned a finite number of initial sets of material parameter values (solution populations) from the search space as input to the FEA model for simulation of a set of shear tests from one animal. The quality of fit of each set of parameters was evaluated based on an objective or cost function to compare the measured force and the FEA predicted solution. The objective function, O_j, was defined in terms of the sum of the squared residuals between the experimental and predicted shear forces for three test directions:

$$O_j = \sum_{d=1}^{3} \sum_{i=1}^{N_{dt}} (F_{di}^{\text{fea}} - F_{di}^{\text{exp}})^2 \tag{15}$$

where O indicated cost function; j was the generation number, for the initial populations, $j=1$; superscripts fea and exp represent finite element analysis and experimental results, respectively. For each set of parameters, three finite element models corresponding to the three shearing directions were run independently. Thus, d indicated one of the three principal shearing directions. N_{dt} was the total number of the time points of experimental data for the d shearing direction.

The running process was stopped when the objective function satisfied the following criterion for four consecutive generations:

$$|O_{j+1} - O_j| \le \Delta, \quad j = m,\ m+1,\ m+2,\ m+3 \tag{16}$$

where Δ was a prescribed specific limit value for the convergence. The optimal material parameters were defined only after satisfying the objective function criterion for four consecutive generations because the process might be trapped at a local minimum for a couple of generations, and a global optimal solution might be missed.

If the convergence criterion for a generation of parameters was not met, the genetic algorithm would iterate to the next generation and create the next solution populations or trial sets of material coefficients via a series of operations. First, values of cost function (fitness) for each parameter set were determined according to Eq. (15) and then used to create offspring. In order to ensure the diversity of the population and reduce the risk of finding local minima, the best solutions of each parameter were modified randomly (mutation). Subsequently, two or more parent individuals were recombined (crossover) for producing one or more descendants. This new generation of parameter sets was used in a finite element model simulation of the same shear test data set. The objective function (Eq. (15)) was evaluated, and the iterative process was automatically repeated until the termination criterion (Eq. (16)) was met.

To accelerate the optimizing computation, a two-step strategy was implemented. First, the numerical program was only fit to the parallel and perpendicular directions to determine five of the six

Table 1 The geometrical dimension of specimens

Exp.	Specimens	Length (mm)	Width (mm)	Height (mm)
A	Parallel	10.04	7.74	1.1
	Perpendicular	12.44	5.84	1.55
	Cross sectional	7.71	5.69	1.85
B	Parallel	10.13	5.5	0.99
	Perpendicular	13.41	6.49	1.05
	Cross sectional	6.8	5.36	2.0

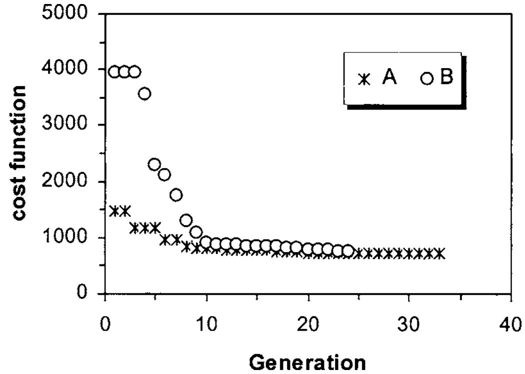

Fig. 5 Variation of cost function with the increase of generation number at the first optimizing step

optimal parameters, C_{10}, g_1, g_2, τ_1, and τ_2, because the fiber reinforcement does not contribute to the response in the parallel or perpendicular shearing directions. Second, the program was fit to all three directions to determine the optimal value of parameter θ in Eq. (3). For the first step, the number of parents (number of population) was set to 100 for the five unknown parameters, and set to 20 parents for the one parameter in the second step. In both steps, the crossover factor or probability was set to 1.0, which indicated all offspring were made by crossover. Usually, the crossover factor is given a value between 0 and 1. A higher crossover factor may yield a faster convergence, if convergence occurs.

The total computation time included the genetic algorithm to evaluate, operate, and generate the material parameters and the finite element analysis simulations. For the present problems, the genetic algorithm portion was fast. Because the recorded displacement was input in the FEA model and contained a lot of noise, the FEA simulation frequently met difficulties in convergence, and the incremental time step size had to be reduced. However, using raw displacement data helped the FEA simulation capture the actual variation of shear force more accurately. Depending on the convergence speed of finite element simulation, it took 10–15 days to iterate to a set of parameters that satisfied Eq. (16) on a Sun Blade 2000 workstation (Solaris 9, dual 900 MHz UltraSPARC III Cu processor, with 6 GB memory) in single CPU mode.

Results

Quality Control Assessment of Test Data. In all, experiments in three shearing directions were performed on each of 15 brainstems. Based on the first rigorous quality control criterion of interfacial testing conditions, Eq. (14), 10 of the 15 experiments were eliminated, which highlighted the experimental challenges of the test protocol.

For the remaining five experiments, the difference between the parallel direction and the perpendicular were assessed. As a result, three of the five remaining experiments were eliminated. Only two experiments, designated A and B, passed both demanding criteria. The geometrical dimensions of the specimens in experiments A and B are provided in Table 1.

Finite Shear Properties. The finite shear properties of 4-week old porcine brainstem were determined using finite element analysis and genetic algorithm method. The experimental data of tests A and B at the strain of 50% in the three shearing directions were used in fitting the transversely isotropic viscoelastic model. The numerical implementation demonstrated good convergence with the increase of generation number (Fig. 5). The specific limit value for convergence, Δ, was set to be 1.0. This value indicated that the relative variation of the cost function was less than 0.2%. In the first optimizing step, the five optimal parameters of $C_{10}(=G_0/2)$, g_1, g_2, τ_1, and τ_2 were obtained at generation 33 and 24 for experiments A and B, respectively. The parameter of θ was optimized in the second step and obtained within five generations for both experiments. The optimal material parameters for each experiment are provided in Table 2.

The average initial shear modulus of brainstem matrix of 4-week old pigs, G_0, was 12.7 Pa. Therefore we concluded that the brainstem offers little resistance to large shear deformations in the parallel or perpendicular directions, due to the dominant contribution of the matrix in these directions. In contrast, the fiber reinforcement stiffness was 121.2 Pa, nearly ten times that of matrix. The viscoelastic characteristics of brainstem were represented using a two-term Prony series (Eqs. (8) and (9)). This form was adopted in order to express short or long relaxation processes. As pointed out by Lanczos [28], this is not a unique representation. The average relative shear relaxation moduli g_1 and g_2 were 0.8973 and 0.0741, respectively. The average characteristic time τ_1 and τ_2 were 0.0047 and 1.4538 s, respectively. The viscoelastic characteristics showed that the shear stress relaxed very rapidly early in the 60 s hold period. In summary, the brainstem is highly anisotropic and viscoelastic, and the axonal fibers have an important role in the tissue response in the cross-sectional shearing direction (Fig. 1).

Predictive Capability of Model. The optimal material parameters were obtained using the genetic algorithm to minimize the error between FEA estimates of shear force at the strain level of 50% and measured values. As expected, for each set of optimal parameters, the FEA estimates of shear force agreed qualitatively with the experimental measurements of shear force obtained at a strain of 50% (Fig. 6). To quantify the agreement, a linear regression was performed between the experimental shear force and the FEA estimate of force. Finite element simulations correlated with experimental results well in all three shearing directions at 50% (Table 3). Specifically, in the parallel and perpendicular directions, all coefficients of determination were above 0.91. In the cross-sectional direction, the coefficients of determination were 0.79 and 0.74 for experiments A and B, respectively.

The predictive capability of the developed model was evaluated by comparing the experimental shear force and FEA solutions. Using the optimal material parameters determined at 50% strain (Table 2), the finite element model was used to simulate all other

Table 2 The material parameters of the brainstem

Exp.	G_0 (Pa)	g_1	g_2	τ_1 (s)	τ_2 (s)	θ (Pa)
A	14.1	0.8634	0.0966	0.0062	0.6207	128.8
B	11.2	0.9313	0.0517	0.0033	2.2868	113.6
Average	12.7	0.8973	0.0741	0.0047	1.4538	121.2

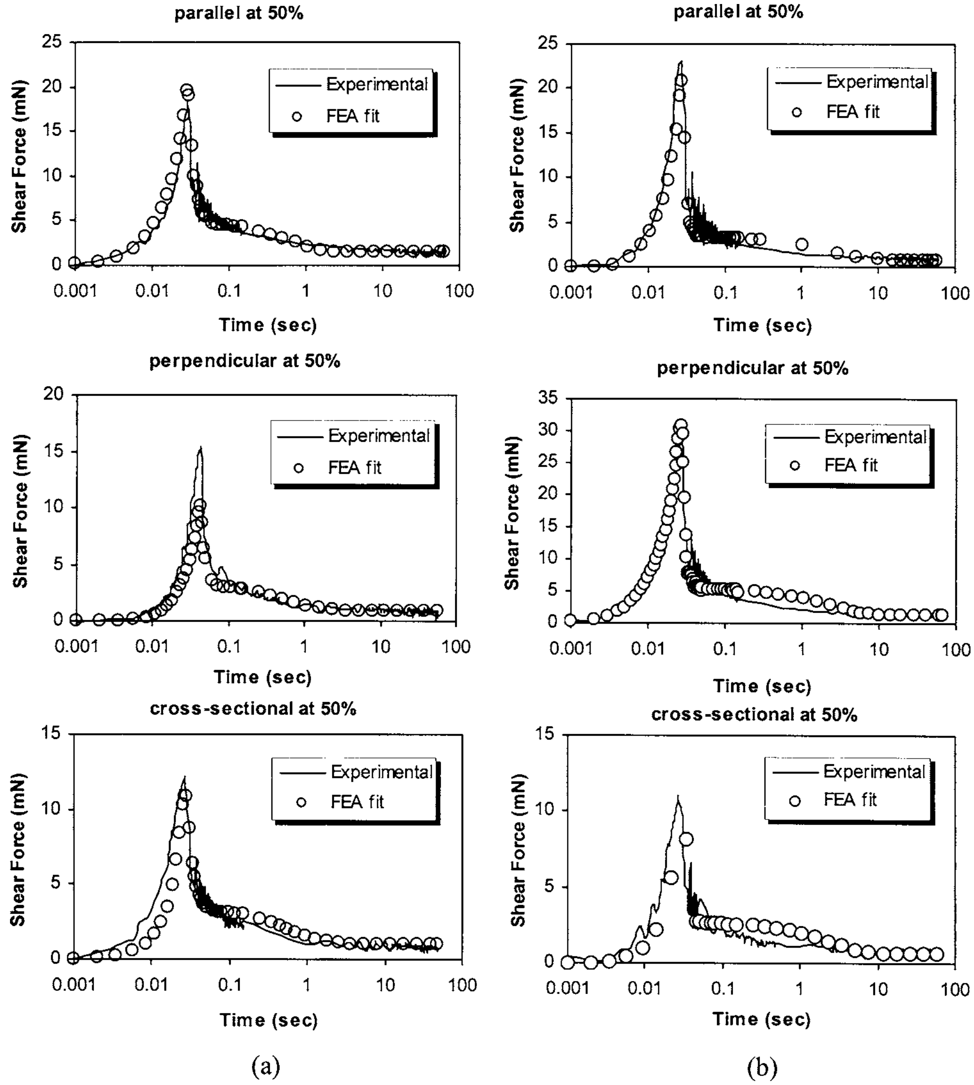

Fig. 6 Fitting results at the strain level of 50% for experiments: (*a*) A and (*b*) B

shear experiments at strain levels 2.5%, 5%, 10%, 20%, 30%, and 40%. The coefficients of determination were all above 71% (Table 3), indicating good predictive capability of the parameter at smaller strains given raw experimental data for comparison.

Discussion

The objective of the current research was to investigate the finite shear properties of the brainstem undergoing large deformation. Shear deformation is associated with the rotational loading due to abrupt deceleration or acceleration of brain, which may lead to diffuse axonal injury, a predominant mechanism of brain injury. If axonal injury occurs in the brainstem, a post-traumatic coma may be induced immediately [29]. Shear stress relaxation test is a suitable experiment to determine the finite shear properties of brain tissues [17,19,30]. Our goal was to study material properties of uninjured tissue to capture reproducible behavior in tissue over a range of strains. In our experiment, engineering shear strain rates reached 25 s^{-1}, which may be associated with mild head injury but does not represent loading conditions for severe head injury. However, the mechanical properties presented here could be used to compare with those in higher strain rate experiments in the future.

The brainstem was modeled as a transversely isotropic, viscoelastic material. Specifically, we represented the brainstem as a

Table 3 Coefficients of determination (R^2) of regression analysis between the experimental shear force and FEA simulated results at strain levels of 2.5–50% for three shearing directions: para (parallel), perp (perpendicular), c-s (cross sectional)

Exp.	Specimens	2.5%	5%	10%	20%	30%	40%	50%
A	para	0.83	0.85	0.82	0.86	0.86	0.89	0.91
	perp	0.86	0.86	0.91	0.92	0.92	0.94	0.95
	c-s	0.74	0.83	0.84	0.85	0.87	0.9	0.79
B	para	0.81	0.82	0.79	0.81	0.87	0.89	0.91
	perp	0.71	0.81	0.78	0.79	0.83	0.86	0.92
	c-s	0.74	0.75	0.8	0.82	0.86	0.84	0.74

fiber reinforced material, similar to the previous linear model which limited its characterization of the brainstem to very small deformations [12]. We described the axonal fibers using a quadratic standard reinforcing strain-energy function and the matrix material using a neo-Hookean model. For simplicity, we assumed that the matrix material and axonal fibers demonstrated similar viscoelastic characteristics.

In the current study, we obtained the finite shear properties of the brainstem of 4-week old pig undergoing large deformation. The axonal fiber initial modulus was 121.2 Pa, which was nearly ten times that of brainstem matrix, 12.7 Pa. For comparison, at small deformations (2.5%), Arbogast and Margulies [12] reported that the real part of the complex modulus of axonal fibers was only three times stiffer than that of the matrix material in adult tissues. Thus, we conclude that the neural fiber component of the brainstem plays a more prominent role at large deformations than at small strains.

Arbogast [31] performed shear stress relaxation tests on adult porcine tissues at 2.5% strain and obtained the long-term shear moduli of brainstem of 180 (±40), 170 (±50), and 200 (±80) Pa in the parallel, perpendicular, and cross-sectional shearing directions, respectively. In contrast, the present study indicates that in the parallel and perpendicular directions the long-term shear modulus of brainstem of 4-week old pig is only 0.36 Pa, equal to that of the brainstem matrix because the fiber does not act in these directions. Examining both the experiment and analysis, we attribute the significant difference between the two studies to preconditioning procedures and deformation magnitudes. In our experiment, two preconditioning runs were performed before data were recorded, whereas no preconditioning was done in Arbogast's experiment [31]. It was shown that the long-term shear modulus of non-preconditioning in vitro brain tissues was 1.53 times that of preconditioning ones on average [32]. Moreover, the long-term modulus of brain tissues is reduced due to the softening effect at large deformations [19].

Previously reported material properties of brain tissues cover a broad range of values, probably due to the variety of test procedures or conditions such as strain rates, strain magnitudes, species, specimen locations and preparations, and loading types. For shear experiments alone, oscillation tests reveal a dynamic elastic modulus range from 600 to 2000 Pa and a dynamic loss modulus range from 350 to 600 Pa [11,12,16,17,25,26,31]. For relaxation tests, adult gray and white matter has an initial shear modulus on the order of 216.5 Pa [19]. Our relaxation tests in brainstem yield much lower values than cerebrum. We measure initial shear modulus values of 12.7 Pa in the parallel and perpendicular shear directions and less than 121.2 Pa in the cross-sectional shear directions. These data demonstrate that the brainstem provides dramatically less resistance to deformations than the cerebrum. Thus, we conclude that the brainstem may be especially vulnerable to distortion during rapid movements of the head.

With a continuum strain energy density function, our model will predict that the stiffness in extension is equivalent to that in compression whereas Miller and Chinzei [15] showed the brain's stiffness in compression is 20% higher than in extension. Examining their test protocol, it is important to note that their specimens were not from a single tissue but composed of arachnoid membrane, gyral white matter and cortical gray matter. As stated by the authors [15], their experimental results represented a spatial averaging behavior of brain tissue because their specimen exhibited composite material stiffness, which depended on many complex factors. Besides, the material orientation was not considered in their experiment. In contrast, our experiment was focused on the carefully oriented specimens of uniform compositions from brainstem. With dissimilar origins of specimens, it is not surprising to find that our results might be different from Miller and Chinzei's experimental results.

Fifteen experiments were performed. In order to ensure that parameters were fit to data from reproducible brain tissue tests, two data quality control criteria were established. The experiments were screened based on the reproducibility at 50% strain and the requirement of equal shear stress in the parallel and perpendicular shearing directions. Previously, Prange and Margulies [19] assessed tissue integrity of samples tested at 50% strain using Nissl staining and found that there was no difference in cell morphology and arrangement between the unstrained tissue and deformed samples. They also verified that the long-term shear modulus at 5% strain was not altered in more than 80% of samples after a sequence of shear tests at strain levels of 2.5%, 5%, 10%, 20%, 30%, 40%, 50%, and then 5% again. In the present study, ten experiments were eliminated because we introduced a condition of reproducibility at 50% strain that had to be satisfied in all three test directions. We justified this rigorous quality control standard because all parameter fitting was performed with the data at 50% strain. The high rejection rate was likely due to slip between the plate and sample given large strains up to 50%. Based on the second data quality control criterion, three of five remaining experiments were eliminated. If the tissue is transversely isotropic, the experimental shear stress in the parallel and perpendicular should be equal since they arise solely from the isotropic matrix. Therefore, it was likely that in the rejected data sets axonal fibers were not precisely oriented with the test direction, either due to the inaccurate excision or orientation in the test apparatus. Ultimately, only two experiments passed both criteria, which highlights the challenges of this brain tissue testing protocol. In addition, because we rejected three of five test data sets, we cannot completely dismiss the possibility that brainstem may not be transversely isotropic, despite its morphology.

Using a transversely isotropic viscoelastic material, the finite element model fit the shear test data at the strain level of 50% well in all three shearing directions. When these material parameters were used to simulate the shear tests at other strain levels, results correlated well with the experimental data, confirming good predictive ability. A neo-Hookean model was employed to describe constitutive response of the matrix. Because neo-Hookean strain-energy function represents a linear response, the consistently excellent fit in the parallel and perpendicular directions where the matrix dominates the response indicates that the deformation of matrix may be considered linear. However, at higher strain levels, the coefficients of determination between measurement and FEA predictions of force in the cross-sectional direction (Table 3) were not as good as in the parallel or perpendicular directions. In undeformed, highly oriented central nervous system tissue, axons are undulated, and they straighten as the tissue is elongated along the axonal axis [18]. This straightening is not uniform but rather may be represented as a population whose variance decreases with stretch. We hypothesize that when the brainstem is subjected to shear deformation in the cross-sectional direction, the axonal deformation is actually inhomogeneous. Future models may be improved using an inhomogeneous model to describe axonal fibers.

To incorporate inhomogeneous deformations of axon fibers into the model, it is necessary to discern the work of fibers both in compression and extension. In the present study, a continuum strain energy density function has been chosen to describe the instantaneous response of the brainstem as a homogeneous, transversely isotropic material. As a result, the tissue response is analyzed as a homogeneous material instead of distinguishing between the response of the matrix and fibers. In the modeling, the assumption of homogeneous deformation of fibers implied that the tissue behaves similarly in compression and extension, which suggested fiber bundles work in compression, although in our experiments, axonal fibers acted only in the cross-section shear direction and mainly experiences stretch. Recently, Miller and Chinzei [15] showed the brain's stiffness in compression is 20% higher than in extension. This result indicated that fibers might work in compression given the fact that brainstem consists of a large portion of fibers, e.g., 90% optic fiber volume fraction in the composites of optic fiber-matrix of adult porcine brainstem [12]. It is not clear how the isotropic matrix could provide higher stiffness in compression than both fibers and matrix in extension. Microstructurally, the embedded fiber bundles in matrix might play a role in resisting compression, but their contribution to the tissue compression stiffness depends on many factors including fiber orientations, fiber bundle buckling stability, specimen dimensions, and fiber-matrix bond strength. Obviously, to fully model inhomogeneous deformations of axonal fibers, experiments should be performed on brainstem to elucidate the work of tissue components in compression.

In nature, most biological soft tissues are anisotropic and viscoelastic. Thus, the material model and parameter estimation technique developed in the current study are likely to find broad applications in characterizing soft tissues such as brain white matter, knee ligaments, and tendons.

Acknowledgment

This work was supported by the Department of Transportation, National Highway Traffic Safety Administration (NHTSA) Grant No. DTNH-22-01-H07551 and by the National Institute Health (NIH) Grant No. R01-NS39679. The authors are grateful to Jill Ralston for her assistance of the animal handling, and Kerry Marder and Dr. Sean Ji for their technical assistance with tissue testing.

Appendix: Transversely Isotropic Hyperelastic Model

If x is the current position of a material particle and $\mathbf{X}$ is the reference position of the same point, the deformation gradient $\mathbf{F}$ is defined as

$$\mathbf{F} = \frac{\partial x}{\partial \mathbf{X}} \tag{A1}$$

The ratio of deformed/undeformed volumes at this point is

$$J = \det(\mathbf{F}) \tag{A2}$$

where $\det(\cdot)$ represents the determinant. A deviatoric deformation gradient is defined to eliminate the volume change for easy finite element implementation of nearly incompressible materials

$$\widetilde{\mathbf{F}} = J^{-\frac{1}{3}}\mathbf{F} \tag{A3}$$

The left and right Cauchy–Green strain tensors are $\widetilde{\mathbf{B}}$ and $\widetilde{\mathbf{C}}$, respectively

$$\widetilde{\mathbf{B}} = \widetilde{\mathbf{F}} \cdot \widetilde{\mathbf{F}}^T, \quad \widetilde{\mathbf{C}} = \widetilde{\mathbf{F}}^T \cdot \widetilde{\mathbf{F}} \tag{A4}$$

Three principal invariants are:

$$\widetilde{I}_1 = \operatorname{tr} \widetilde{\mathbf{B}} = \operatorname{tr} \widetilde{\mathbf{C}} \tag{A5}$$

$$\widetilde{I}_2 = \tfrac{1}{2}[(\operatorname{tr} \widetilde{\mathbf{B}})^2 - \operatorname{tr}(\widetilde{\mathbf{B}}^2)] = \tfrac{1}{2}[(\operatorname{tr} \widetilde{\mathbf{C}})^2 - \operatorname{tr}(\widetilde{\mathbf{C}}^2)] \tag{A6}$$

$$\widetilde{I}_3 = \det\widetilde{\mathbf{B}} = \det\widetilde{\mathbf{C}} \tag{A7}$$

If the unit vector $\mathbf{a}_0$ is the direction of the fiber reinforcement in an undeformed configuration, two additional invariants that involve $\mathbf{a}_0$ and $\widetilde{\mathbf{C}}$ are defined to describe the effect of the fiber-reinforcement [20]

$$\widetilde{I}_4 = \mathbf{a}_0 \cdot \widetilde{\mathbf{C}} \cdot \mathbf{a}_0, \quad \widetilde{I}_5 = \mathbf{a}_0 \cdot \widetilde{\mathbf{C}}^2 \cdot \mathbf{a}_0 \tag{A8}$$

In order to describe the nonlinear response of transversely isotropic, hyperelastic materials, an uncoupled strain-energy function per unit volume is defined in terms of the five invariants

$$W(\widetilde{I}_1,\widetilde{I}_2,\widetilde{I}_3,\widetilde{I}_4,\widetilde{I}_5) = W_{\text{iso}}(\widetilde{I}_1,\widetilde{I}_2,J) + W_{\text{aniso}}(\widetilde{I}_4,\widetilde{I}_5) \tag{A9}$$

where $W_{\text{iso}}(\widetilde{I}_1,\widetilde{I}_2,J)$ describe the response of the isotropic matrix; and the $W_{\text{aniso}}(\widetilde{I}_4,\widetilde{I}_5)$ describe the directional contribution of the fiber reinforcement. It is implicitly assumed that the fibers respond only to stretch in their direction, and their response acts in their direction only.

For hyperelastic materials, the second Piola–Kirchhoff stress is [20,21]

$$\boldsymbol{\tau} = 2J^{-\frac{2}{3}}\mathrm{DEV}\left(\frac{\partial W}{\partial \widetilde{\mathbf{C}}}\right) - pJ\mathbf{C}^{-1} \tag{A10}$$

where

$$\mathrm{DEV}[\cdot] = [\cdot] - \frac{1}{3}([\cdot]:\widetilde{\mathbf{C}})\widetilde{\mathbf{C}}^{-1}, \quad p = -\frac{\partial W}{\partial J} \tag{A11}$$

p is the hydrostatic pressure. Equation (A10) may be further written as

$$\boldsymbol{\tau} = 2J^{-\frac{2}{3}}\mathrm{DEV}\left[\sum_{\alpha}\left(\frac{\partial W}{\partial \widetilde{I}_\alpha}\frac{\partial \widetilde{I}_\alpha}{\partial \widetilde{\mathbf{C}}}\right)\right] - pJ\mathbf{C}^{-1}, \quad \alpha = 1,2,4,5 \tag{A12}$$

where

$$\frac{\partial \widetilde{I}_1}{\partial \widetilde{\mathbf{C}}} = \mathbf{I}, \quad \frac{\partial \widetilde{I}_2}{\partial \widetilde{\mathbf{C}}} = \widetilde{I}_1\mathbf{I} - \widetilde{\mathbf{C}} \tag{A13}$$

$$\frac{\partial \widetilde{I}_4}{\partial \widetilde{\mathbf{C}}} = \mathbf{a}_0 \otimes \mathbf{a}_0, \quad \frac{\partial \widetilde{I}_5}{\partial \widetilde{\mathbf{C}}} = \mathbf{a}_0 \otimes \widetilde{\mathbf{C}} \cdot \mathbf{a}_0 + \mathbf{a}_0 \cdot \widetilde{\mathbf{C}} \otimes \mathbf{a}_0 \tag{A14}$$

where $\mathbf{I}$ is an identity tensor.

The Cauchy stress tensor of a transversely isotropic, compressible hyperelastic material is

$$\begin{aligned}\boldsymbol{\sigma} &= \frac{2}{J}\,\mathrm{dev}\left(\widetilde{\mathbf{F}}\frac{\partial W}{\partial \widetilde{\mathbf{C}}}\widetilde{\mathbf{F}}^T\right) - p\mathbf{I} \\ &= \frac{2}{J}\,\mathrm{dev}[(W_1 + \widetilde{I}_1W_2)\widetilde{\mathbf{B}} - W_2\widetilde{\mathbf{B}}^2 + \widetilde{I}_4W_4\mathbf{a}\otimes\mathbf{a} \\ &\quad + \widetilde{I}_4W_5(\mathbf{a}\otimes\widetilde{\mathbf{B}}\cdot\mathbf{a} + \mathbf{a}\cdot\widetilde{\mathbf{B}}\otimes\mathbf{a})] - p\mathbf{I}\end{aligned} \tag{A15}$$

where

$$W_\alpha = \partial W/\partial \widetilde{I}_\alpha, \quad \mathrm{dev}[\cdot] = [\cdot] - \tfrac{1}{3}([\cdot]:\mathbf{I})\mathbf{I}, \quad \mathbf{a} = \mathbf{F}\mathbf{a}_0 \tag{A16}$$

$\mathbf{a}$ denotes the configuration of $\mathbf{a}_0$ during the deformation.

If the material is incompressible, $I_3 = J^2 = 1$, W is a function of only I_1, I_2, I_4, and I_5, but an arbitrary Lagrangian multiplier p is introduced as a reaction stress to the kinematics constraint of incompressibility on the deformation field.

In Eq. (A15), the Cauchy stress $\boldsymbol{\sigma}$ actually consists of two components: the equivalent pressure p and the deviatoric stress $\mathbf{S}$

$$p = -\tfrac{1}{3}\mathbf{I}:\boldsymbol{\sigma}, \quad \mathbf{S} = \boldsymbol{\sigma} + p\mathbf{I} \tag{A17}$$

References

[1] Sosin, D. M., Sniezek, J. E., and Waxweiler, R.J., 1995, "Trends in Death Associated With Traumatic Brain Injury, 1979 Through 1992. Success and Failure," J. Am. Med. Assoc., **273**, pp. 1778–1780.
[2] Thurman, D. J., Alverson, C., Dunn, K. A., Guerrero, J., and Sniezek, J. E., 1999, "Traumatic Brain Injury in The United States: A Public Health Perspective," J. Head Trauma Rehabil., **14**, pp. 602–615.
[3] Center of Disease Control, 1990, "Childhood Injuries in the United States," Am. J. Dis. Child, **144**, pp. 627–646.
[4] Lee, M., Melvin, J., and Ueno, K., 1987, "Finite Element Analysis of Traumatic Subdural Hematoma," *Proc. of 31st Stapp Car Crash Conference*.
[5] Margulies, S., Thibault, L., and Gennarelli, T., 1990, "Physical Model Simulations of Brain Injury in The Primate," J. Biomech., **23**, pp. 823–836.
[6] Meaney, D., Smith, D., Ross, D., and Gennarelli, T., 1995, "Biomechanical Analysis of Experimental Diffuse Axonal Injury," J. Neurotrauma, **12**, pp. 311–322.
[7] Mendis, K., 1992, "Finite Element Modeling of the Brain to Establish Diffuse Axonal Injury Criteria," Ph.D. dissertation, Ohio State University.
[8] Miller, R., Margulies, S., Leoni, M., Nonaka, M., Chen, X., Smith, D., and Meaney, D., 1998, "Finite Element Modeling Approaches for Predicting Injury

in an Experimental Model of Severe Diffuse Axonal Injury," *Proc. of Proceedings of 42nd Stapp Car Crash Conference*.
[9] Zhou, C., Khalil, T., and King, A., 1995, "A New Model Comparing Impact Responses of the Homogeneous and Inhomogeneous Human Brain," *Proc. of 39th Stapp Car Crash Conference*.
[10] Jellinger, K., 1983, "Secondary Brainstem Involvement in Blunt Head Injury," *Advance in Neurotraumatology*, Elsevier, Princeton.
[11] Arbogast, K., and Margulies, S., 1998, "Material Characterization of the Brainstem From Oscillatory Shear Tests," J. Biomech., **31**, pp. 801–807.
[12] Arbogast, K., and Margulies, S., 1999, "A Fiber-Reinforced Composite Model of the Viscoelastic Behavior of the Brainstem in Shear," J. Biomech., **32**, pp. 865–870.
[13] Miller, K., and Chinzei, K., 1997, "Constitutive Modeling of Brain Tissue: Experiment and Theory," J. Biomech., **30**, pp. 1115–1121.
[14] Miller, K., Chinzei, K., Orssengo, G., and Bednarz, P., 2000, "Mechanical Properties of Brain Tissue In-Vivo: Experiment and Computer Simulation," J. Biomech., **33**, pp. 1369–1376.
[15] Miller, K., and Chinzei, K., 2002, "Mechanical Properties of Brain Tissue in Tension," J. Biomech., **35**, pp. 483–490.
[16] Darvish, K., and Crandall, J., 2001, "Nonlinear Viscoelastic Effects in Oscillatory Shear Deformation of Brain Tissue," Med. Eng. Phys., **23**, pp. 633–645.
[17] Brands, D., Peters, G., and Bovendeerd, P., 2004, "Design and Numerical Implementation of a 3-D Non-Linear Viscoelastic Constitutive Model for Brain Tissue During Impact," J. Biomech., **37**, pp. 127–134.
[18] Meaney, D., 2003, "Relationship Between Structural Modeling and Hyperelastic Material Behavior: Application to CNS White Matter," Biomech. Model. Mechanobiol., **1**, pp. 279–293.
[19] Prange, M., and Margulies, S., 2002, "Regional, Directional, and Age Dependent Properties of the Brain Undergoing Large Deformation," ASME J. Biomech. Eng., **124**, pp. 244–252.
[20] Spencer, A. J. M., 1984, *Theory of the Mechanics of Fiber-Reinforced Composites*, Springer-Verlag, New York.
[21] Weiss, J. A., Maker, B. N., and Govindjee, S., 1996, "Finite Element Implementation of Incompressible, Transversely Isotropic Hyperelasticity," Comput. Methods Appl. Mech. Eng., **135**, pp. 107–128.
[22] Hibbit, Karlsson, & Sorensen, Inc., 2003, ABAQUS *Theory Manual Version 6.3*.
[23] Merodio, J., and Ogden, R. W., 2003, "Instabilities and Loss of Ellipticity in Fiber-Reinforced Compressible Non-Linearly Elastic Solids Under Plane Deformation," Int. J. Solids Struct., **40**, pp. 4707–4727.
[24] Merodio, J., and Ogden, R. W., 2005, "Mechanical Response of Fiber-Reinforced Incompressible Non-Linearly Elastic Solids," Int. J. Non-Linear Mech., **40**, pp. 213–227.
[25] McElhaney, J., Roberts, V., and Hilyard, J., 1976, *Handbook of Human Tolerance*, Japan Automobile Research Institute, Tokyo.
[26] Arbogast, K., Thibault, K., Pinheiro, B., Winey, K., and Margulies, S., 1997, "A High-Frequency Shear Device for Testing Soft Biological Tissues," J. Biomech., **30**, pp. 757–759.
[27] Storn, R., and Price, K., 1997, "Differential Evolution—A Simple and Efficient Heuristic for Global Optimization Over Continuous Spaces," J. Global Optim., **11**, pp. 341–359.
[28] Lanczos, C., 1956, *Applied Analysis*, Prentice-Hall, Englewood Cliffs, NJ.
[29] Smith, D., Nonaka, M., Miller, R., Leoni, M., Chen, X., Alsop, D., and Meaney, D., 2000, "Immediate Coma Following Inertia Brain Injury Dependent on Axonal Damage in the Brainstem," J. Neurosurg., **93**, pp. 315–322.
[30] Bilston, L. E., Liu, Z., and Phan-Thien, N., 2001, "Large Strain Behavior of Brain Tissue in Shear: Some Experimental Data and Differential Constitutive Model," Biorheology, **38**, pp. 335–345.
[31] Arbogast, K., 1997, "A Characterization of the Anisotropic Mechanical Properties of The Brainstem," Ph.D. dissertation, University of Pennsylvania.
[32] Gefen, A., and Margulies, S., 2004, "Are In Vivo and In Situ Brain Tissues Mechanically Similar?," J. Biomech., **37**, pp. 1339–1352.